Pulse-Based Analog VLSI Velocity Sensors

Jörg Kramer, Rahul Sarpeshkar, and Christof Koch

***Abstract*—We present two algorithms for estimating the velocity of a visual stimulus and their implementations with analog circuits using CMOS VLSI technology. Both are instances of so-called token methods, where velocity is computed by identifying particular features in the image at different locations; in our algorithms, these features are abrupt temporal changes in image irradiance. Our circuits integrate photoreceptors and associated electronics for computing motion onto a single chip and unambiguously extract bidirectional velocity for stimuli of high and intermediate contrasts over considerable irradiance and velocity ranges. At low contrasts, the output signal for a given velocity tends to decrease gracefully with contrast, while direction-selectivity is maintained. The individual motion-sensing cells are compact and highly suitable for use in dense 1-D or 2-D imaging arrays.**

***Index Terms*— Analog CMOS, analog VLSI, machine vision, motion sensors, photoreceptors, smart vision chips, velocity sensors.**

I. Introduction

VARIOUS APPLICATIONS in automotive guidance, robotics, and remote sensing require sensors for processing visual motion that are small, consume little power, and work in real time. Real-time operation is necessary whenever a system has to interact with a dynamic environment. Considering the type of environments humans are typically exposed to, we shall use the term "real time" in its common anthropocentric meaning, i.e., for time delays not exceeding a few tens of milliseconds. Because motion algorithms are computationally expensive, techniques in which they can be implemented in parallel are very attractive. Parallel implementations become particularly appealing if image sensing and motion computation can be combined within one stage, so that sensors estimating the optical flow throughout a scene in real time can be conveniently integrated on a single chip. Such *smart-vision* chips could be used in stand-alone applications, such as tracking cars, or as front-ends in conventional machine-vision systems [1], [2].

Because image irradiance is a continuous function of time, asynchronous circuit implementations are preferable to clocked implementations. The latter introduce temporal aliasing artifacts that can significantly compromise time-sensitive computations, such as those associated with optical flow.

Analog processing is more economic in terms of silicon area and power than digital processing of comparable complexity and thus makes higher pixel densities possible. Its main drawback is its lack of precision, but high-precision motion processing is often not possible anyway, because of noisy input data and fundamental computational problems associated with the estimation of the velocity field from the optical flow [3].

We present here two analog VLSI motion circuits that operate in the subthreshold domain [4], based on neuromorphic principles [5]. We believe that our circuits can be used as building blocks for large and very dense "optical flow" chips. Part of the work described here has been presented at a conference [6].

II. Review of Analog VLSI Motion Sensors

Algorithms for motion sensing can be divided into two main categories [3], [7]. In *intensity*-based methods the image irradiance, or some filtered version of it, is directly used to estimate the optical flow on a dense map. The two most popular types of intensity-based motion algorithms are *gradient* and *correlation* methods. Both methods suffer from the fact that estimating optical flow is at the very least a numerically ill-conditioned and frequently an ill-posed problem [8], [9]. The second major class of motion algorithms are known in computer vision as *token*-based methods and are associated in the psychophysical literature with *long-range* motion. They first extract particular features from the image, such as edges, corners, or higher-level features, estimating velocity in a subsequent stage at sparse locations throughout the image by tracking these features across time. The key difficulty with methods working on discrete space or time intervals (or both) is known as the *correspondence* problem: which feature at a given time or location corresponds to which feature at a different time or location.

In the following, we review previously-built analog VLSI motion sensors that incorporate the photoreceptors and the processing circuitry on a single chip:

Some early implementations used intensity-based methods. Among the first circuits operating on a gradient algorithm was an "optical mouse" chip for estimating a uniform velocity in two dimensions [10].[1] Under an orthogonal projection system, uniform velocity corresponds to global translation of a rigid object space relative to the sensor. The circuit consisted of an 8×8 array of velocity sensors. Offset effects of individual

Manuscript received May 2, 1995; revised April 1, 1996. This work was supported by grants from the Swiss National Science Foundation, the Office of Naval Research, the Center for Neuromorphic Systems Engineering as a part of the National Science Foundation Engineering Research Center Program, and by the Office of Strategic Technology of the California Trade and Commerce Agency. This paper was recommended by Associate Editor L. R. Carley.

J. Kramer and R. Sarpeshkar are with the Computation and Neural Systems Program, California Institute of Technology, Pasadena, CA 91125 USA.

C. Koch is with the Division of Biology, California Institute of Technology, Pasadena, CA 91125 USA.

Publisher Item Identifier S 1057-7130(97)01163-4.

[1] For an even earlier design of an "optical mouse" on a single chip using a token-based method with digital logic see [11].

pixels were reduced by averaging across the array. The circuit only gave a sensible output for high-contrast edges, and even then showed poor performance. This disappointing result was mainly due to the discrepancy between the high-precision requirement of the algorithm (requiring temporal and spatial derivatives) and the low precision of the analog circuitry.

Due to the intrinsic difficulty of computing derivatives using low precision hardware [12], some of the subsequent work has concentrated on implementing correlation methods, originally proposed as models for motion perception systems of insects [13], since they show superior numerical stability. A 1-D spatial-correlation sensor was built, where a spatially-filtered version of the input signal was fed into a circuit that multiplied the delayed signal of one pixel with the undelayed signal of the adjacent pixel on either side [14]. The correlation signals for each direction were averaged along the array and used to interpolate displacements in the subpixel range. A modified version of this sensor in a 2-D array, where the delay circuit was replaced with a sample-and-hold circuit and the multiplication with an absolute difference, provided motion signals along two orthogonal directions [15]. Recently, an adaptive 1-D correlation system was implemented to model the motion adaptation in the visual system of the fly [16]. It correlated a low-pass-filtered and a high-pass-filtered version of the input signal from adjacent pixels, whereby the common cut-off frequency of the two filters was slowly adapted to the frequency of the input signal.

Since purely correlation-based methods yield output signals that depend on contrast and illumination, as well as on velocity, general interest has shifted toward methods that first extract low-level image features as tokens for further processing. All of the circuits described here identify rapid temporal brightness transients as temporal edges or sharp spatial brightness gradients as spatial edges.

Motion sensors with token-based inputs and correlation-type motion computation include a 27 pixel 1-D array inspired by the auditory system of barn owls [15]. This chip propagated voltage pulses, triggered by temporal edges, through delay lines. Pulses from adjacent pixels were propagated through parallel delay lines from opposite directions. The velocity of an edge stimulus was extracted from the position of their meeting point. A 2-D scheme, implemented as a hexagonal array of 26 $\times$ 26 pixels [18] compared the velocity of temporal edges traveling across the image plane with the preset velocity of pulses propagating through delay lines. The above-mentioned model for motion perception of insects [13] was also applied to image tokens [19]. Using a spatial edge detector, that was constructed with two resistive grids to approximate a difference-of-Gaussians operator [20], as input stage, it performed a binary correlation of delayed and undelayed voltage pulses from adjacent pixels, respectively.

While such correlation-based algorithms are interesting models of how motion computations are carried out in neurobiological circuits, they do not represent commercially attractive velocity sensors, since they are usually tuned to a particular velocity or to a narrow velocity range. For some of them, the output signal is strongly dependent on the contrast of the visual stimulus or too sensitive to circuit parameters.

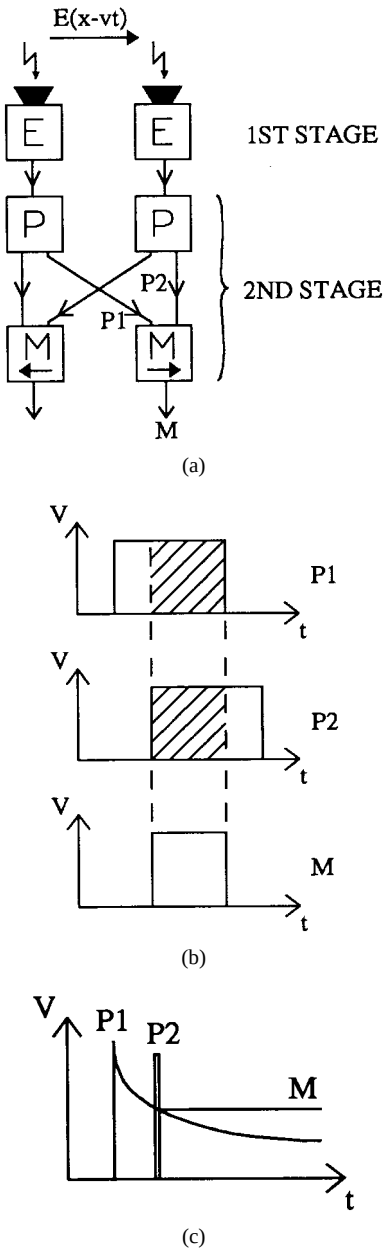

Fig. 1. Architecture and output signals of the two motion sensors. (a) Schematic diagram of the motion sensing principle. Temporal edge detectors (E) generate current pulses in response to fast irradiance (i.e., brightness) transients. Pulse-shaping circuits (P) convert the current pulses into voltage pulses. Voltage pulses from adjacent pixels are fed into direction-selective motion circuits (M) computing velocity in one dimension for both directions of motion. Each motion circuit responds to velocity in one direction of motion only. (b) Voltage pulses of the facilitate-and-trigger (FT) motion sensor. The width of the output pulse of the motion circuit (M) equals the overlap time of the facilitation pulse (P_1) and the trigger pulse (P_2), if the facilitation pulse precedes the trigger pulse. If the trigger pulse precedes the facilitation pulse, no output pulse is generated. The width of the output pulse thus encodes velocity in one direction of motion. (c) Voltage signals of the facilitate-and-sample (FS) motion sensor. The analog output voltage of the motion circuit (M) equals the voltage of the slowly decaying facilitation pulse (P_1) at the time of arrival of the thin sampling pulse $(P2)$. If the sampling pulse precedes the facilitation pulse, the output voltage is low. The analog output voltage thus encodes velocity in one direction of motion.

Some token-based methods measure the time of travel of an image token between two fixed locations, which is inversely related to the velocity. A circuit inspired by a model for one-dimensional direction-selectivity in the rabbit

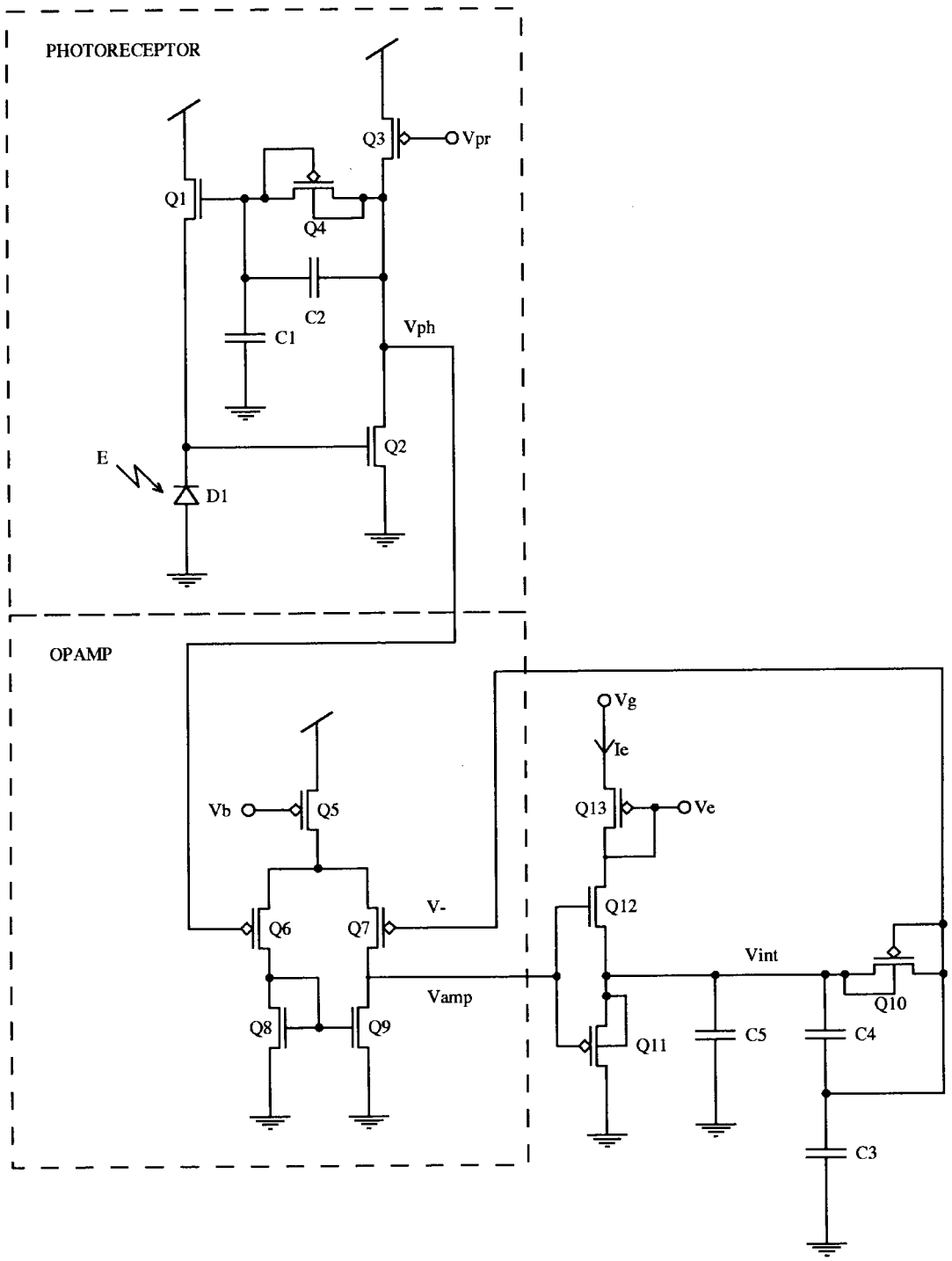

Fig. 2. Circuit diagram of the temporal edge detector. The adaptive photoreceptor described in [27] responds to a change dE in irradiance E with a voltage step $dV_{\rm ph}$ that only depends on contrast dE/E. The photoreceptor is coupled to a circuit for amplification, differentiation, and rectification (Q_5–Q_{13}, C_3–C_5), that converts a positive voltage step $dV_{\rm ph}$ into a current pulse I_e.

retina [21] was implemented as a 2-D array of 47 $\times$ 41 pixels [22]. Inhibitory connections between neighboring pixels in one direction suppressed the response for motion in that direction, called the null direction. In the other direction, the preferred direction, pulses were triggered by temporal edges and terminated by inhibition from the neighboring pixel. For low speeds and contrasts, however, the pulse amplitudes and widths were strongly dependent on speed and contrast and the pulses decayed before inhibition set in. Another time-of-travel algorithm was implemented in a 5×5 array [23]. It used a spatial edge detector and measured the time the thresholded edge signal spent on each pixel for two orthogonal directions. Direction-selectivity was obtained by correlating the temporal derivatives of the edge signal at adjacent pixels. This chip operated over three orders of magnitude of speed and for a wide contrast range. However, it only worked for sharp edges, had problems with fixed-pattern noise and light sensitivity of the processing circuitry, and sometimes showed

spurious responses in the null direction for edges near the contrast threshold [24]. An improved version of this circuit was implemented in a 1-D array with 9 pixels [24]. A scheme that generated a binary output pulse based on the times of disappearance of spatial edge signals from neighboring pixels and a preset time constant was implemented in a 23×23 array [25]. The direction of motion was obtained from the edge signal at a third pixel. Every pixel yielded two output pulses tuned to different velocities along each of three directions, but the relation between velocity and output-pulse duration was ambiguous. Furthermore, the output signals were read by scanners, so that the information on pulse duration could only be obtained by integrating the scanned signals over time. An implementation of a 1-D array with 8 elements measured the time of travel of temporal edges between neighboring pixels, using an inhibition signal from a third pixel to implement direction-selectivity [26]. The motion-sensing elements were very compact and the system encoded velocity robustly and with low fixed-pattern noise over two orders of magnitude in speed and illumination and over a wide contrast range.

III. Circuit Architecture

In this paper, two elementary analog VLSI motion sensors for the determination of 1-D velocity in real time are reported and analyzed. They exhibit a monotonic dependence of the output signal on the measured velocity and operate robustly over large speed and illumination ranges. They are more compact and respond to lower contrasts than most previous implementations. Their circuit architecture derives from the structure of the underlying token-based time-of-travel motion algorithm and can be conceptually divided into two separate stages, a feature extraction stage and a velocity computation stage (Fig. 1(a)). In the first stage, rapid temporal changes in the image irradiance are converted into thin current pulses by "temporal edge detectors" (E) at two nearby locations on the chip. In the second stage, these current pulses are transformed into voltage pulses by pulse-shaping circuits (P), which are fed into a pair of direction-selective motion circuits (M), *each responding to one direction of motion*. The details of the second stage differ significantly among the two motion sensors, while the same edge detector is used for both of them.

The *facilitate-and-trigger* (FT) motion circuit measures the overlap time of binary pulses of a given width produced by the two adjacent pulse-shaping circuits, as shown in Fig. 1(b) [19]. The *facilitate-and-sample* (FS) motion circuit samples a time-varying voltage pulse generated by one pulse-shaping circuit with a thin voltage spike generated by an adjacent pulse-shaping circuit, as shown in Fig. 1(c) [6]. For each FT or FS motion circuit, one pulse (P_1) acts as a facilitation pulse or timing pulse, while the other pulse (P_2) initiates the measurement of speed at the instant of its onset. Direction-selectivity is obtained because each motion circuit responds only if P_1 precedes P_2.

Note that a single motion sensing element in a 1-D array contains a pair of motion circuits, but only one edge detector and one pulse-shaping circuit, because the pulses are shared among neighboring motion circuits.

IV. Temporal Edge Detector

The temporal edge detector used for both motion circuits converts a rapid increase in brightness into a current pulse. This corresponds to detection of temporal dark-bright or so-called ON edges. A current pulse is also triggered if the illumination over the entire chip changes simultaneously (light flicker). The circuit schematic is shown in Fig. 2.

The adaptive photoreceptor $(D_1, Q_1\text{–}Q_4, C_1, C_2)$ is described in [27]. Its output voltage $V_{\rm ph}$ increases logarithmically with irradiance of the photodiode D_1, as long as the MOSFET's are operated below threshold. Thus, a transient dE in the image irradiance E causes a voltage transient $dV_{\rm ph}$ that is only a function of contrast dE/E. This property is highly desirable for the extraction of local features from an image, because the overall illumination of a scene is likely to change with time. The transient step response is higher than the adapted dc response by $(C_1 + C_2)/C_2$, the inverse of the capacitive divider gain in the feedback loop. The *I–V* relationship of the adaptive element Q_4 is that of a sinh. Consequently, the adaptation is slow for small output voltage steps and fast for large steps. With $(C_1 + C_2)/C_2 = 10$, adaptation time constants of several seconds were obtained. In subthreshold operation, the transient change of the photoreceptor output voltage to an irradiance step is given by

$$dV_{\rm ph} = \left(\frac{C_1 + C_2}{C_2}\right)\left(\frac{kT}{q\kappa}\right)\left(\frac{dE}{E}\right) \tag{1}$$

where kT/q is the thermal voltage and κ is the back-gate coefficient of Q_1.

The output of the photoreceptor is fed into a circuit that transduces positive voltage excursions in the photoreceptor voltage, corresponding to ON edges, to a current. The transistors Q_5–Q_9 constitute an operational amplifier with a bias V_b, connected to some other transistors $(Q_{10}$–$Q_{13})$ and capacitors $(C_3$–$C_5)$, so that it is in a noninverting feedback configuration. The capacitors C_3 and C_4 form a capacitive divider that causes the transient gain of $V_{\rm int}$ to be $(C_3{+}C_4)/C_4$ with respect to the input voltage $V_{\rm ph}$ of the amplifier. The adaptive element Q_{10} is a sinh element, identical to that used in the photoreceptor, that prevents the V_- node of the amplifier from floating by slowly adapting it to $V_{\rm int}$. The current charging the node $V_{\rm int}$ is given by

$$I_e = C_{\rm tot}\frac{dV_{\rm int}}{dt} \tag{2}$$

where

$$C_{\rm tot} = C_5 + \frac{C_3 C_4}{C_3 + C_4} \tag{3}$$

and where we make the assumption that Q_{10} is only weakly turned on, and also that the excursion of $V_{\rm amp}$ is large enough to open either Q_{11} or Q_{12}. Detection of an ON edge causes I_e to be positive, supplied by Q_{12}, whereas detection of an OFF edge causes it to be negative, supplied by Q_{11}. The transistor Q_{11} is source-connected to minimize body-effects, since the dc voltages of operation are around 1.5 V. Choosing to detect

ON edges only, we sense the current in Q_{12} with the diode-connected Q_{13} and use V_e to mirror copies of it to succeeding circuits. The voltage V_g sets the gain of this output mirror if it is operated within a few mV of V_{DD}. The circuit thus serves as a differentiating, amplifying, and half-wave-rectifying element all-in-one. It is a functional analog of auditory hair cells that senses the motion of the basilar membrane in the cochlea. Here, this circuit is used to sense voltage changes in the photoreceptor output caused by irradiance increases. As long as Q_{12} is completely turned on, i.e., during sufficiently large ON edge transients, we can calculate the magnitude of the resulting output current pulse from (1) and (2) as

$$I_e = C_{\text{tot}}\left(\frac{C_3+C_4}{C_4}\right)\left(\frac{C_1+C_2}{C_2}\right)\left(\frac{kT}{q\kappa}\right)\left(\frac{1}{E}\frac{dE}{dt}\right). \quad (4)$$

The output current I_e of the edge detector is then proportional to the temporal contrast $(\frac{1}{E}\frac{dE}{dt})$, which is the product of the velocity v and the spatial contrast $(\frac{1}{E}\frac{dE}{dx})$, i.e.,

$$\frac{1}{E}\frac{dE}{dt} = \frac{v}{E}\frac{dE}{dx}. \quad (5)$$

V. Pulse-Shaping Circuits

In both motion sensors, the output of the temporal edge detector feeds into a pulse-transduction stage. The FT motion sensor uses a nonlinear filtering circuit to convert the current pulse from the edge detector into a thin voltage spike that is translated into a voltage pulse of fixed amplitude and width by a refractory neuron circuit. The FS motion sensor uses the same nonlinear filter to convert the current pulse from the edge detector into two signals, a thin voltage spike and a slowly decaying voltage signal. The nonlinear filtering and refractory neuron circuits are described in the following subsections.

A. Nonlinear Filter

The circuit shown in Fig. 3(a) is a nonlinear version of a differentiator consisting of a source-follower-like low-pass filter $(Q_3$–$Q_5, C)$ in the feedback path of a high-gain amplifier (Q_1, Q_2). The input to the circuit is a current I_{in} proportional to I_e (cf. (4)), obtained from the mirror formed by connecting the output voltage of the edge detector (V_e in Fig. 2) to V_{in} of the filtering circuit. In response to an input current pulse, two voltage signals are generated: The voltage V_f produces a sharp spike, while the voltage V_s responds with a sharp onset and a $\log(t)$-like decay. The input I_{in} may be thought of as an impulse that sets the initial condition on the diode-capacitor subcircuit of Q_4, Q_5, and C. It may be shown that, for an initial condition with a pulse amplitude of I_o, the diode-capacitor current I_{out} is given by

$$I_{\text{out}}(t) = \frac{I_o}{1+\frac{I_o t}{CV_K}} \quad (6)$$

where

$$V_K = \frac{kT(\kappa+1)}{q\kappa^2}. \quad (7)$$

The voltage V_K obtained by using two stacked diodes is larger than that obtained by using one diode, and serves to increase V_f and V_s. After a sufficiently long time t, such that $I_o t \gg CV_K$, $I_{\text{out}}(t) = CV_K/t$,

$$V_s(t) \sim V_K \log(t) \quad (8)$$

and both I_{out} and V_s are independent of I_o and therefore of temporal edge contrast [according to (4)].

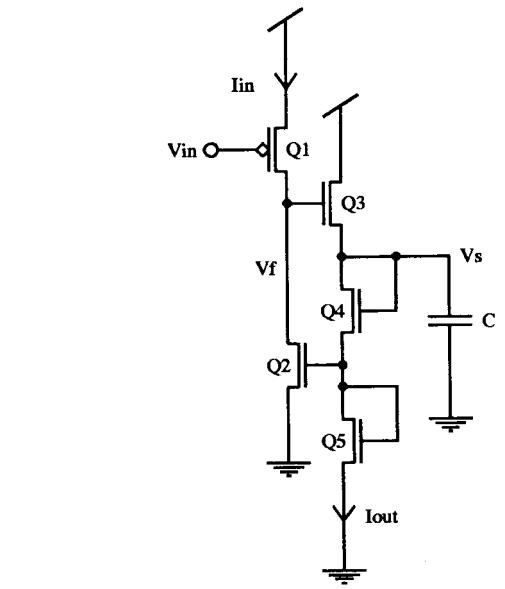

(a)

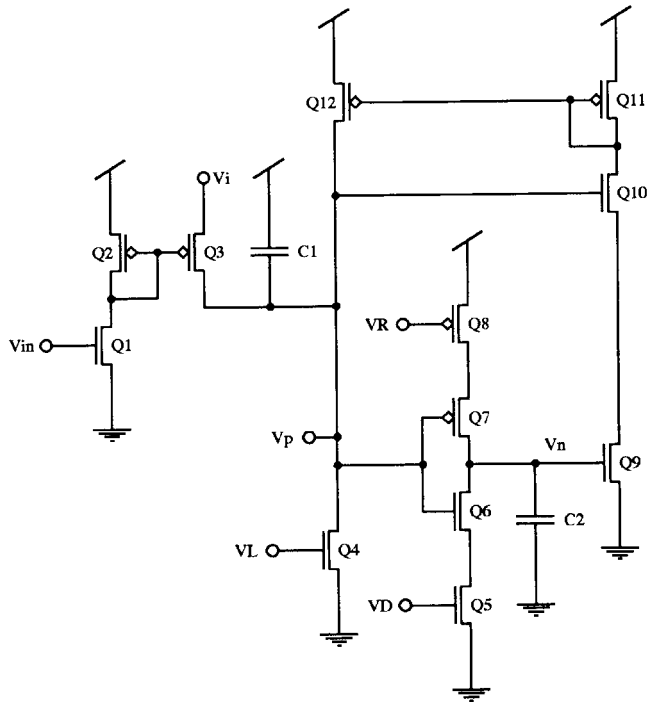

(b)

Fig. 3. Circuit diagrams of the pulse-shaping circuits. (a) Nonlinear filter generating a thin voltage pulse V_f and a slowly decaying voltage pulse V_s in response to a current pulse I_{in} that is a mirror copy of I_e of the temporal edge detector. The pulse-shaping circuit of an FS motion sensor comprises just this nonlinear filter. (b) Refractory neuron generating a voltage pulse V_p of fixed width and amplitude in response to a voltage spike V_{in}. The pulse-shaping circuit of an FT motion sensor uses a nonlinear filter whose output V_f is coupled to the input V_{in} of a refractory neuron.

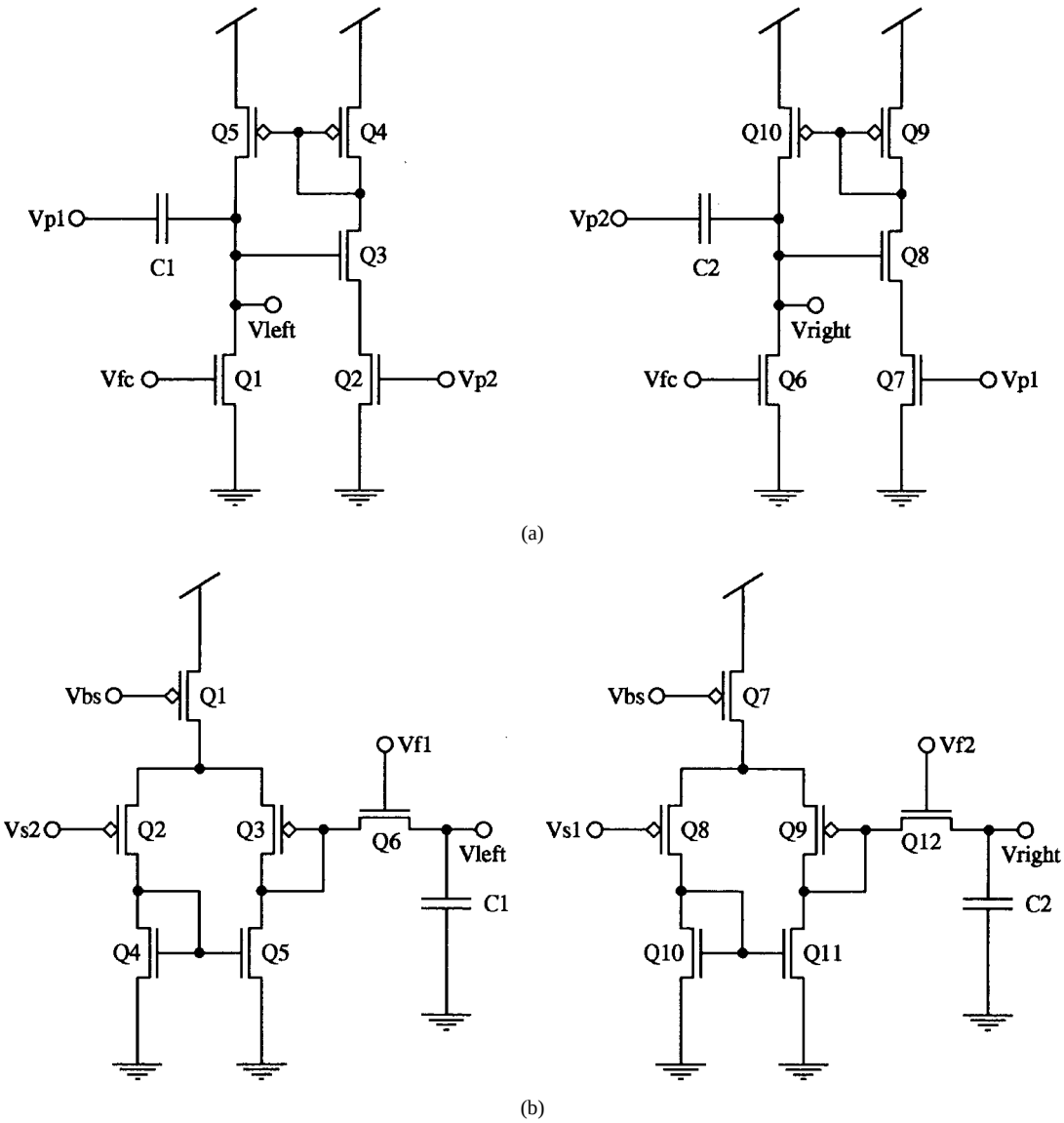

Fig. 4. Circuit diagrams of pairs of motion cells for opposite directions. (a) FT. The voltage terminals V_{p1} and V_{p2} are coupled to the outputs of adjacent refractory neuron circuits. An output pulse $V_{\rm left}$ is triggered if the onset of V_{p2} precedes the onset of V_{p1} and an output pulse $V_{\rm right}$ is triggered if the onset of V_{p1} precedes the onset of V_{p2}. (b) FS. The voltage terminals V_{f1} and V_{s1} are coupled to the outputs of one nonlinear filter, while V_{f2} and V_{s2} are coupled to those of an adjacent one. The sampled output voltage $V_{\rm left}$ is high if the onset of V_{s2} precedes V_{f1} and the sampled output voltage $V_{\rm right}$ is high if the onset of V_{s1} precedes V_{f2}.

Note that the circuit does not have an explicit threshold for the value of I_o where contrast-insensitivity begins. Neither does V_s have an explicit time constant determined by a bias voltage, since a diode-capacitor configuration intrinsically adapts to time constants over many orders of magnitude.

B. Refractory Neuron

In the FT sensor, the refractory neuron circuit shown in Fig. 3(b) converts voltage spikes V_f from the nonlinear filter (Fig. 3(a)) into digital voltage pulses V_p of fixed width. The circuit is based on a simple model for a sodium-leak neuron of biological nervous systems. It is explained in detail in [28]. Here we only provide a brief description: The voltage V_p represents the membrane potential and rests at ground. The voltage V_n represents the state of activation of the sodium conductance modeled by Q_5–Q_{12} and rests at V_{DD}. The bias voltage V_L sets the leak current through Q_4. The bias voltage V_D sets the pulsewidth of the output pulse. The bias voltage V_R sets the refractory period of the neuron or the minimum time between output pulses. The capacitor C_1 represents the membrane capacitance, and C_2 represents the capacitance needed to store the state of activation of the sodium conductance. All bias voltages and currents are set in the subthreshold region of operation.

VI. Experimental Results

Both motion sensors were fabricated using a 2 μm n-well CMOS process provided by the MOSIS prototyping service.[2] The chips were shielded from light by a metal layer with

[2]MOSIS (MOS Implementation System), Information Sciences Institute of the University of Southern California, Marina del Rey, CA.

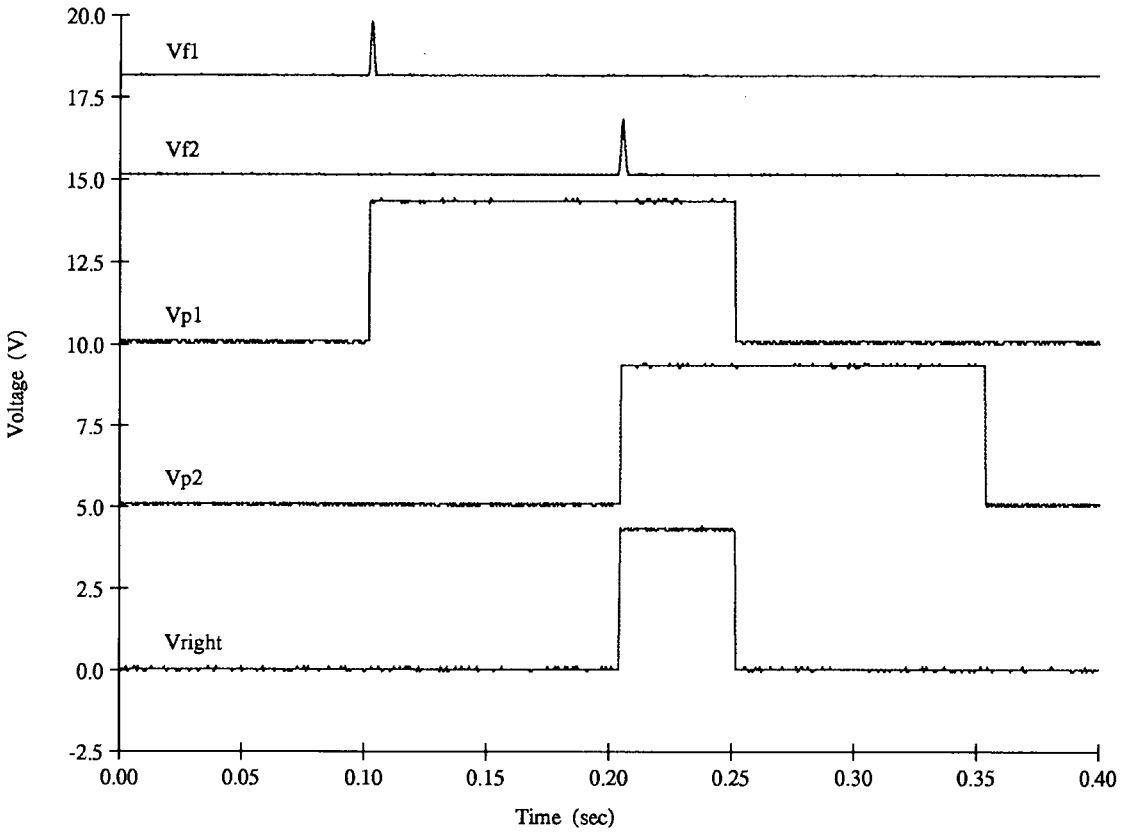

(a)

Fig. 5. Output voltage traces of different stages of analog VLSI implementations of the FT and FS motion algorithms. The waveforms show the responses of the circuits to a sharp, moving, black-to-white ON edge under ac-incandescent room illumination. Both motion sensors were fabricated using a standard 2-μm n-well CMOS process available through MOSIS, with 300 μm spacing between the photoreceptors. (a) FT. V_{f1} and V_{f2} are the thin output spikes of the nonlinear filters signaling the detection of a sharp rise in image irradiance at adjacent pixels. V_{p1} and V_{p2} are the output voltage pulses of the refractory neurons in response to V_{f1} and V_{f2}, respectively. Their width is tunable by a bias voltage and was set to 148 ms. For the preferred direction, V_{p1} is the facilitation pulse and V_{p2} is the trigger pulse. $V_{\rm right}$ is the output pulse in the preferred direction. For better visibility, the voltage traces for V_{f1}, V_{f2}, V_{p1}, and V_{p2} are offset by 18, 15, 10, and 5 V, respectively. The output pulsewidth of 47 ms corresponds to an image speed of 6.4 mm/s on the chip.

(24 μm)^2 openings for the photodiodes. A pixel spacing of $\Delta x = 300$ μm was chosen.

Suppose V_p is at ground and V_n is at V_{DD}, their respective resting potentials. If V_p is caused to rise by a thin current spike through Q_1–Q_3, greater than the leak current, to a voltage greater than V_L, then the current through Q_9–Q_{12} will be greater than the leak current. A positive feedback action occurs that forces V_p to then rise very rapidly to V_{DD}. However, with V_p at V_{DD}, V_n starts to be discharged through Q_5 and Q_6. When V_n is discharged below V_L, the current through Q_9–Q_{12} falls below the leak current and a positive feedback action occurs that causes the leak current to discharge V_p to ground. When V_p is at ground, Q_7 and Q_8 recharge V_n back to V_{DD} and the neuron is reset to its resting state.

The transistors Q_1–Q_3 are responsible for converting a voltage spike V_f from the nonlinear filter into a current spike that is input to the neuron. Note that in order for the input current to generate a pulse in the neuron, the voltage spike must have a sufficiently large amplitude so that the charging current exceeds the leak current, and it must be sufficiently wide so that C_1 is charged to a voltage that is greater than V_L. This condition sets an edge-contrast threshold for the FT motion circuit.

VII. Motion Circuits

A. Facilitate-and-Trigger

The FT motion sensor was originally proposed in [19], but was not implemented at the time. It is an improvement upon the delay-and-correlate algorithm presented in the same paper in that it exhibits a *monotonic* dependence of the output pulsewidth on the velocity.[3] In the FT scheme, pulses triggered by an edge signal at two adjacent pixels are timed against each other, leading to an inverse relationship between output pulsewidth and speed, as is observed for the motion algorithm described in [23]. Direction-selectivity is obtained by making the motion circuit sensitive to the order of arrival of the two pulses.

The FT motion circuit receives its inputs from two pulse-shaping circuits that transduce current pulses from adjacent edge detectors E_1 and E_2 into voltage pulses V_{p1} and V_{p2} of fixed amplitude and width. The two FT motion circuits responding to opposite directions of motion are schematically

[3]The delay-and-correlate algorithm is based on a model of motion perception in insects [13] and exhibits a *nonmonotonic* dependence of the pulsewidth on the velocity.

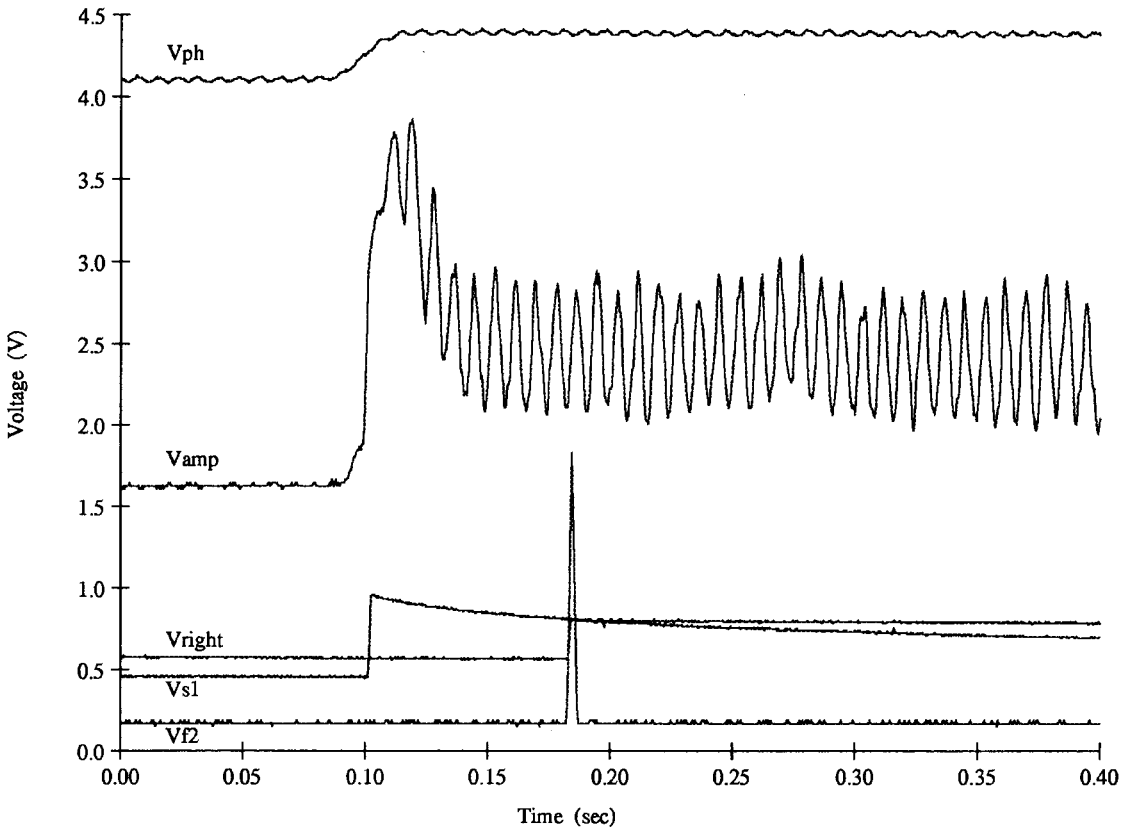

(b)

Fig. 5. *(Continued)*. Output voltage traces of different stages of analog VLSI implementations of the FT and FS motion algorithms. The waveforms show the responses of the circuits to a sharp, moving, black-to-white ON edge under ac-incandescent room illumination. Both motion sensors were fabricated using a standard 2-μm n-well CMOS process available through MOSIS, with 300-μm spacing between the photoreceptors. (b) Edge detector and FS. $V_{\rm ph}$ is the photoreceptor output and $V_{\rm amp}$ the output of the operational amplifier of an edge detector. V_{s1} is the slowly decaying facilitation pulse of the nonlinear filter, initiated at the rising edge of $V_{\rm ph}$ and $V_{\rm amp}$, V_{f2} is the thin sampling pulse triggered by the arrival of the irradiance transient at the adjacent edge detector in the preferred direction of V_{s1} and V_{f2}. $V_{\rm right}$ is the sampled output voltage. For better visibility, the $V_{\rm ph}$ trace and the $V_{\rm amp}$ trace are offset by 3 and 1 V, respectively. Note that the flicker noise of the room lighting can clearly be seen on the $V_{\rm ph}$ and $V_{\rm amp}$ traces. The 82 ms delay of V_{f2} with respect to the onset of V_{s1} corresponds to an image speed of 3.65 mm/s on the chip.

shown in Fig. 4(a). In the first circuit $(Q_1$–$Q_5, C_1)$ the pulse V_{p2} opens Q_2, thereby setting a time window within which an output pulse $V_{\rm left}$ can be triggered by opening Q_3 through capacitive coupling of the onset of the pulse V_{p1}. As long as Q_2 is open, its current is mirrored by Q_4 to Q_5 and $V_{\rm left}$ stays high. With the termination of V_{p2} the current through Q_5 is shut off and $V_{\rm left}$ goes low due to the leak current through Q_1 set by V_{fc}. The pulse V_{p2} therefore serves as a facilitation pulse for the triggering of an output pulse by V_{p1}. The width of the output pulse $V_{\rm left}$ equals the temporal overlap of the facilitation pulse V_{p2} and the trigger pulse V_{p1}, if the facilitation pulse precedes the trigger pulse. If V_{p1} arrives before V_{p2}, the output stays low, because at the onset of V_{p1}, Q_2 is off, so that Q_4 and Q_5 are also off and Q_1 discharges any capacitive current from V_{p1}. Note that the falling edge of V_{p1} does not couple in either, since Q_1 prevents $V_{\rm left}$ from going below ground. The first circuit thus only responds to motion from E_2 to E_1.

The second circuit $(Q_6$–$Q_{10}, C_2)$ uses V_{p1} as facilitation pulse and V_{p2} as trigger pulse and therefore responds to motion from E_1 to E_2. A traveling edge therefore activates only one of the motion circuits depending on its direction of motion.

The width of the output pulse is

$$\tau = u\Theta(u) \tag{9}$$

with $u = T - \Delta x/v$, where T denotes the width of the neuron pulse, Δx the pixel spacing, v the velocity of the edge signal, and $\Theta(\cdot)$ the Heaviside function. There is no output for very low speeds, when the travel time $\Delta x/v$ of the edge between two pixels is longer than the facilitation pulse. The circuit has its highest sensitivity $d\tau/dv$ at small τ, corresponding to the lowest detectable velocities. The sensitivity is proportional to v^{-2}, i.e., the sensitivity is high within a limited velocity range and flattens out toward higher velocities.

B. Facilitate-and-Sample

The FS motion algorithm was designed to yield a monotonic response curve showing high sensitivity over a larger velocity range than the FT algorithm [6].

The FS motion circuit receives its inputs from two pulse-shaping circuits that transduce current pulses from adjacent edge detectors E_1 and E_2 into pairs of voltage pulses. Each pulse-shaping circuit [the nonlinear filter of Fig. 3(a)] generates a thin spike (V_{f1} or V_{f2}) and a slowly decaying signal (V_{s1}

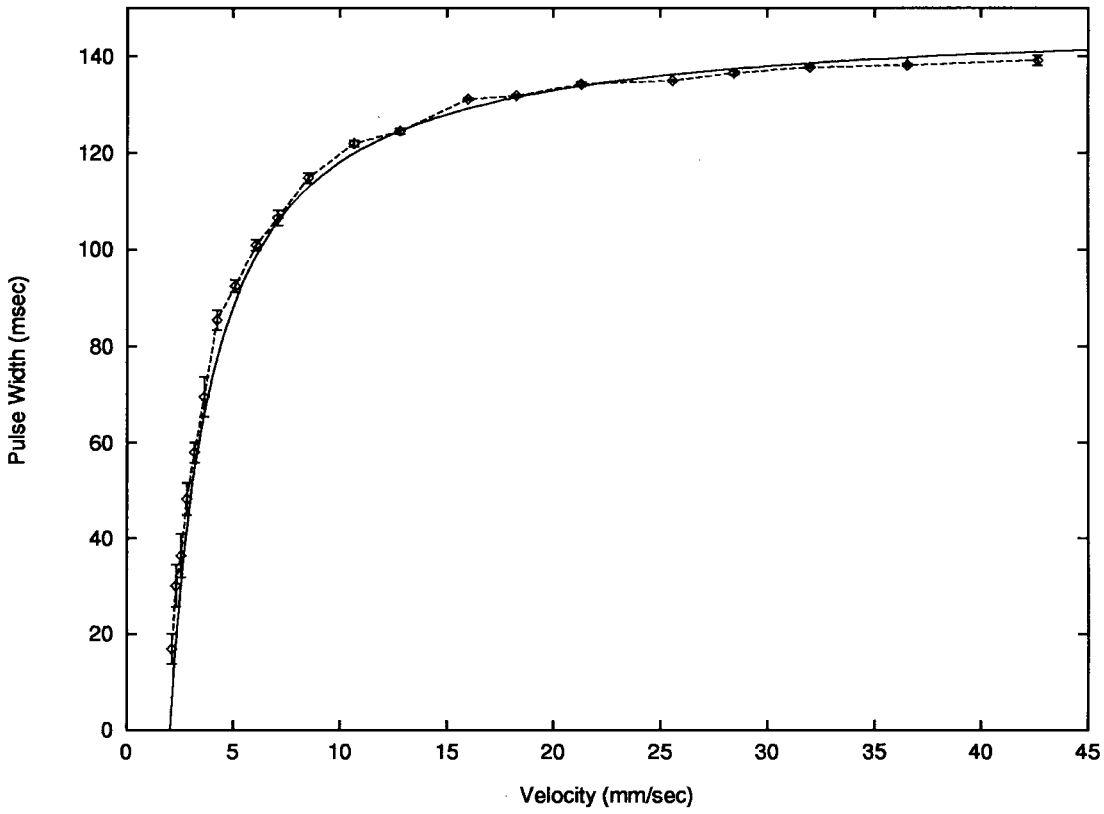

(a)

Fig. 6. Output signals of motion sensing elements for the preferred direction ofmotion of a sharp black-to-white ON edge versus image velocity for ac-incandescent room illumination with theoretical fits. The pixel spacing of 300 μm corresponds to an optical angle of 1.28° and a distance of 8.5 mm on the object. The object was imaged from a distance of 380 mm using a lens with a focal length of 13 mm. Each data point represents the average of 5 successive measurements, the error bars indicate rms errors computed from the data. (a) FT. The data confirms the inverse dependence of the output pulsewidth on the velocity of the theoretical fit, as obtained from (9) with a neuron pulsewidth of 148 ms, corresponding to a minimum detectable velocity of 2 mm/s on the chip.

or V_{s2}). The two FS motion circuits responding to opposite directions of motion are schematically shown in Fig. 4(b). They are standard sample-and-hold circuits. In the first circuit $(Q_1$–$Q_6, C_1)$, the slowly-decaying pulse V_{s2} initiated at E_2 is sampled by the thin voltage spike V_{f1} triggered at E_1. If the facilitation pulse V_{s2} precedes the sampling pulse V_{f1}, the sampled analog voltage V_{left} is a measure of the time delay between the onset of V_{s2} and V_{f1}. If the sampling pulse arrives before the facilitation pulse, the facilitation pulse triggered by the preceding edge is sampled, which has decayed to a low voltage, unless edges arrive in quick succession. The first circuit thus senses motion from E_2 to E_1. The monotonic decay of the facilitation pulse ensures unambiguous encoding of speed in the sampled voltage.

In the second circuit $(Q_7$–$Q_{12}, C_2)$, the slowly-decaying pulse V_{s1} initiated at E_1 is sampled by the thin voltage spike V_{f2} triggered at E_2. The second circuit therefore senses motion from E_1 to E_2.

It follows from the discussion of the nonlinear filter that if we assume

$$I_o \frac{\Delta x}{v} \gg C V_K \tag{10}$$

then the sampled output voltage V_{out}, corresponding to V_{left} or V_{right} in Fig. 5(b), is independent of I_o and given by

$$V_{\text{out}} \sim V_K \log\left(\frac{\Delta x}{v}\right). \tag{11}$$

The FS circuit responds down to very low speeds, while showing better sensitivity at high speeds than the FT circuit. This is because the decay time constant of the facilitation pulse, being based on diode-capacitor dynamics, increases with time, i.e., adapts to the measured delay, whereas the output pulsewidth of the FT cell decreases with delay at a fixed rate. The sensitivity dV_{out}/dv of the FS curve is highest at low speeds, but it only decays as v^{-1} in contrast with the v^{-2} dependence of the FT curve.

For quantitative measurements, sheets of paper with printed gray-scale patterns were wrapped around a rotating drum to provide the optical stimuli. The stimuli were projected onto the chip from a distance of 380 mm by means of a Fairchild Cinphar lens with a focal length $f = 13$ mm and an f-number of 1.8. Unless otherwise noted, measurements were taken under ac-incandescent room-lighting conditions, where a white paper surface provided an illuminance of about 1.2 lux on the chip. The input and output pulses of the FT motion circuit in response to a black-white ON edge are plotted in Fig. 5(a). For the same edge stimulus, Fig. 5(b) shows the signals at different stages of the edge detector, the input pulses to the FS motion circuit from the pulse-shaping circuits, and the sampled output

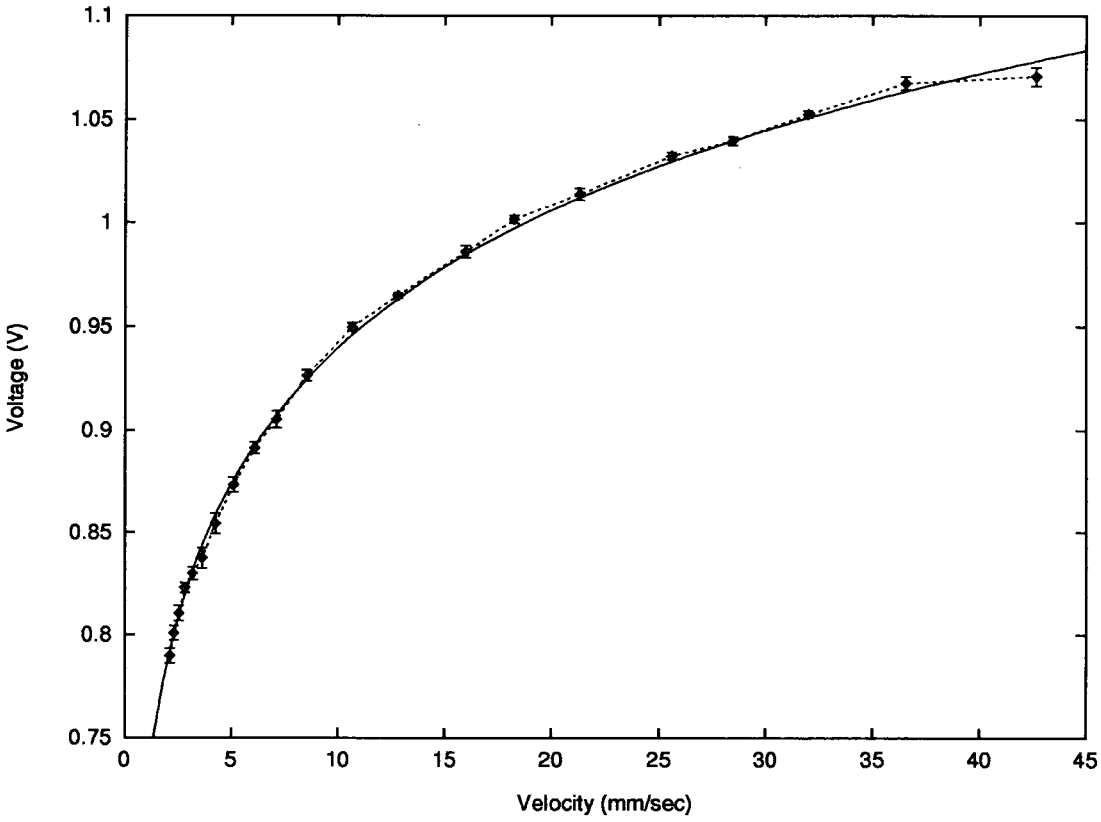

(b)

Fig. 6. *(Continued)*. Output signals of motion sensing elements for the preferred direction of motion of a sharp black-to-white ON edge versus image velocity for ac-incandescent room illumination with theoretical fits. The pixel spacing of 300 μm corresponds to an optical angle of 1.28° and a distance of 8.5 mm on the object. The object was imaged from a distance of 380 mm using a lens with a focal length of 13 mm. Each data point represents the average of 5 successive measurements, the error bars indicate rms errors computed from the data. (b) FS. The dependence of the analog output voltage on the velocity matches the logarithmic relationship predicted by the theoretical fit according to (11), allowing velocity measurements down to very low speeds. Note that data is taken over the same range of speeds for the FT and FS motion sensing elements.

voltage. The 120 Hz flicker noise can clearly be seen on the output voltage trace $V_{\rm amp}$ of the operational amplifier of the edge detector. The bias of the amplifier was set to a low gain (low V_b) so that the flicker noise remained tolerable.

Fig. 6(a) and (b) shows the response to the same ON edge as a function of the velocity of its image on the chip in the preferred direction, together with a theoretical fit according to (9) and (11) for the FT and FS motion sensors, respectively. For both circuits, the measured data agrees well with the fits. The fit for the FT response assumes an output pulsewidth of the refractory neuron of $T = 148$ ms. Since the maximum detectable delay is equal to the facilitation pulsewidth, the minimum detectable speed amounts to $v_{\rm min} = \frac{\Delta x}{T} = 2$ mm/s. The maximum speed $v_{\rm max}$ is limited by the ability of the FT motion sensor to discriminate between the order of arrival of pulses from adjacent edge detectors, which depends on the stimulus, the rise times of the neuron pulses and the dynamics of the motion circuits. The rise times of the neuron pulses and of the output pulses of the motion circuits for the ON edge were measured to be around 200 ns. We therefore assume that $v_{\rm max}$ is five or six orders of magnitude higher than $v_{\rm min}$ for the chosen neuron pulsewidth, exceeding the velocity range of the rotating drum stimulus by far. The null direction shows no response at all for speeds smaller than $v_{\rm max}$, as long as the temporal edge separation is sufficiently large.

In the FS circuit, the voltage sampled in the null direction depends on the time interval between succeeding edge pulses. In the absence of spatial aliasing, all measured values for the null direction are smaller than those for the preferred direction. The maximum velocity $v_{\rm max}$ for correct operation of the FS motion sensor is limited by the finite width of the sampling pulse. If the velocity of an edge traveling in the null direction is too high, the sampling pulse in the null direction overlaps the facilitation pulse and the sampled voltage is high, exceeding the one for the preferred direction. The black-white ON edge results in a pulsewidth of 2.5 ms [see V_{f2} trace in Fig. 5(b)], yielding a maximum image velocity of $v_{\rm max} = 300$ μm/2.5 ms = 120 mm/s for the given setup. The minimum detectable velocity $v_{\rm min}$ is determined by light-induced leak currents, that cause V_s to decay to ground after several seconds, depending on the illumination level.

The response curves of the FT and FS circuits to the ON edge at different global illumination levels are shown in Fig. 7(a) and (b), respectively. The proximity of the curves to each other is a result of the contrast encoding of the photoreceptor. The response of the FS circuit at high speeds starts to decrease with illumination under dim room-lighting conditions. This is due to bandwidth limitation of the photoreceptor circuit at low irradiance levels [29]. With increasing speed, the height of the current pulses at the output of the edge detector becomes

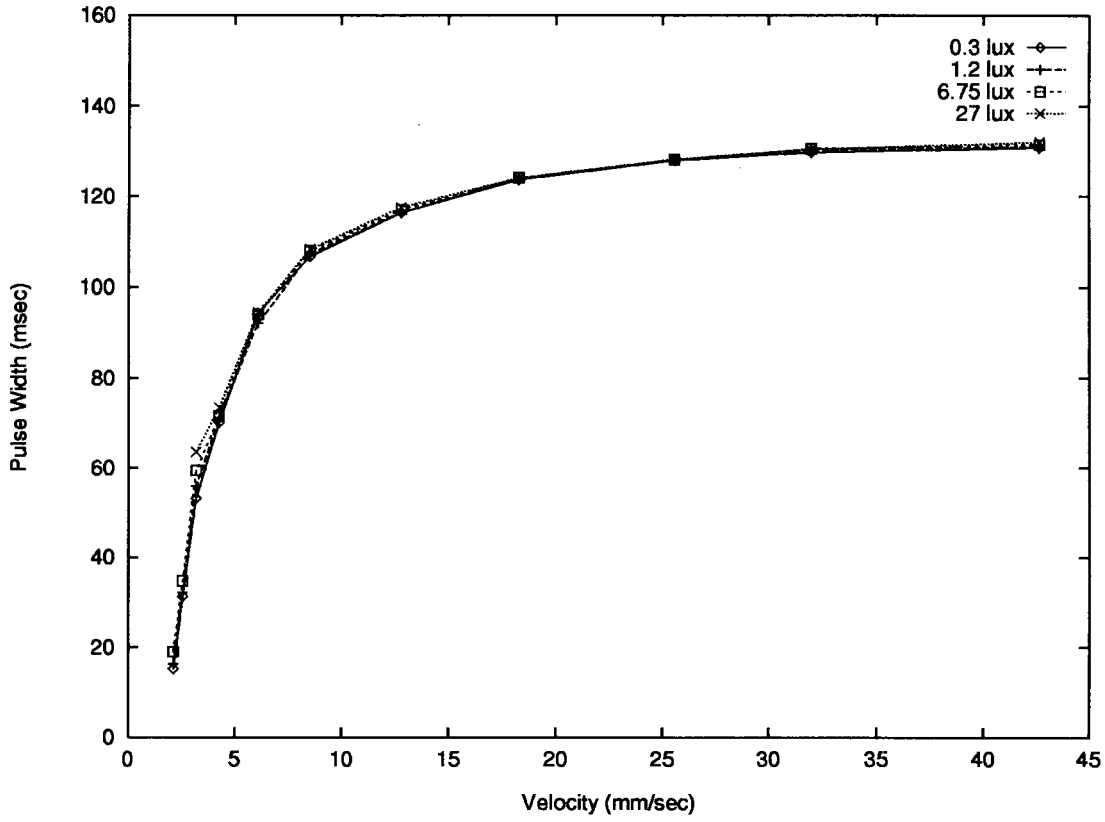

(a)

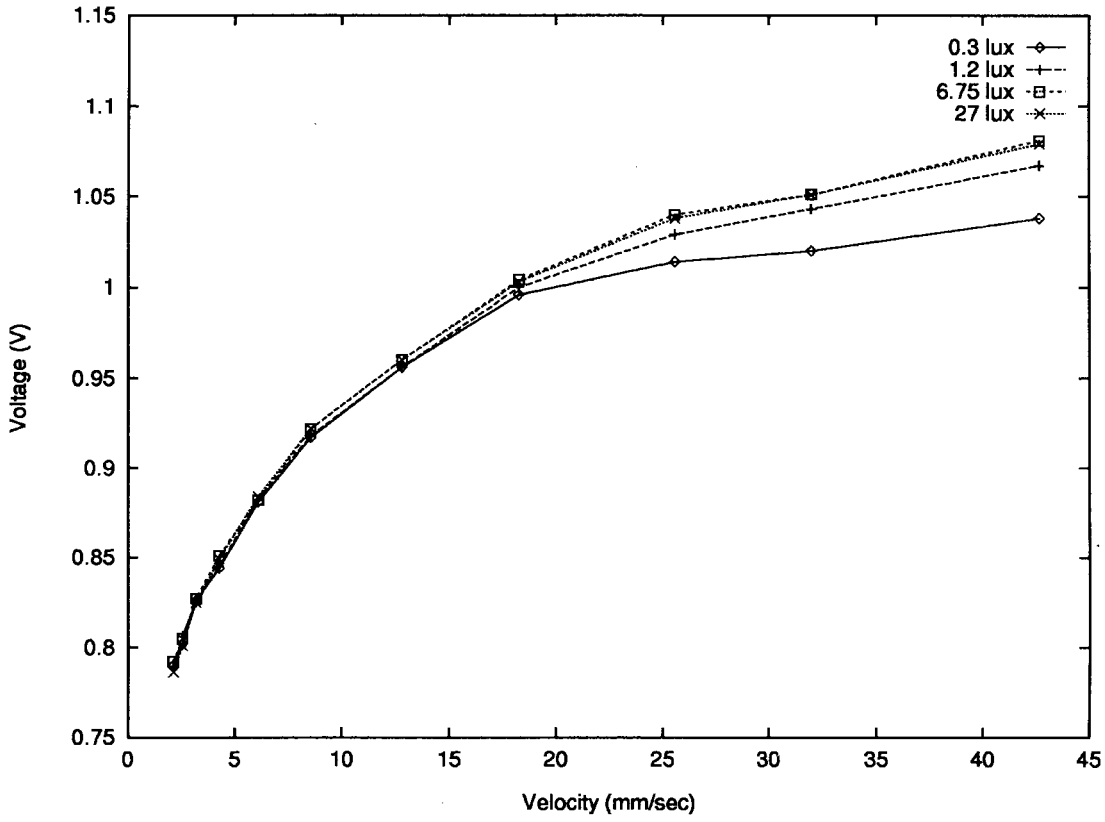

(b)

Fig. 7. Output signal of a motion sensing element for the preferred direction of motion of a sharp black-to-white ON edge versus image velocity for different ac-incandescent room illumination levels. Each data point represents the average of 5 successive measurements. (a) FT. (b) FS.

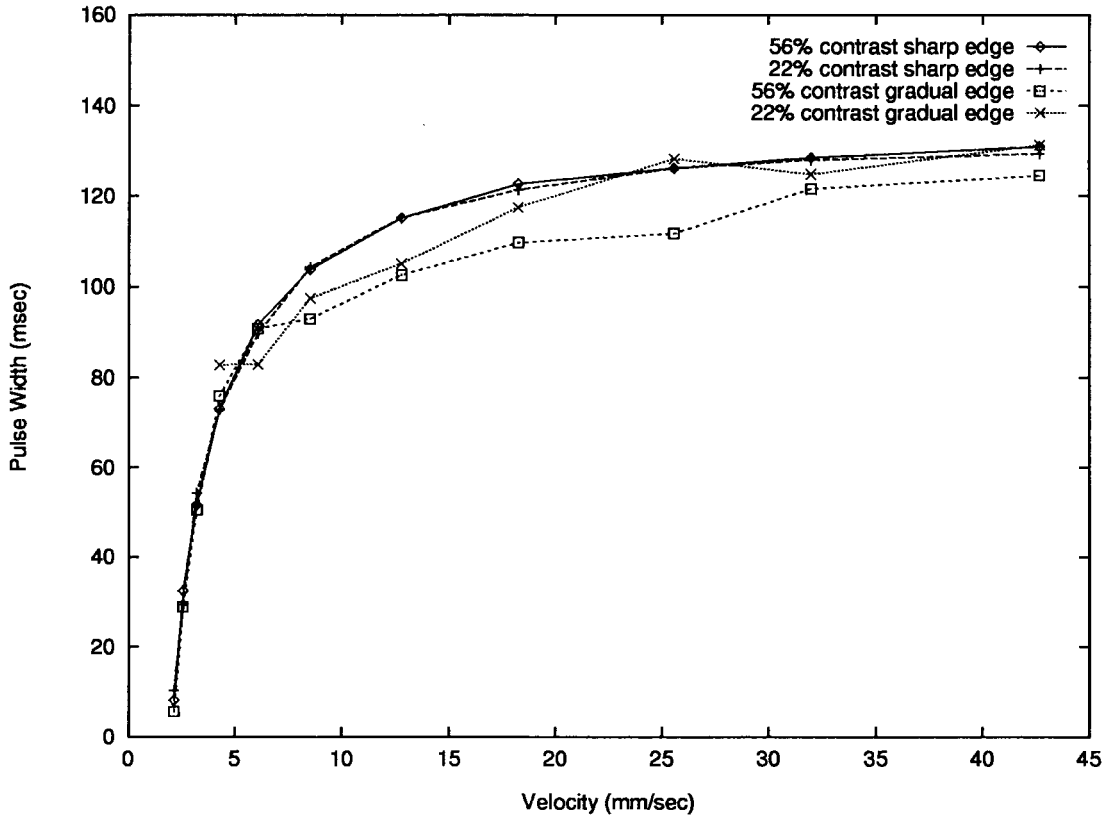

(a)

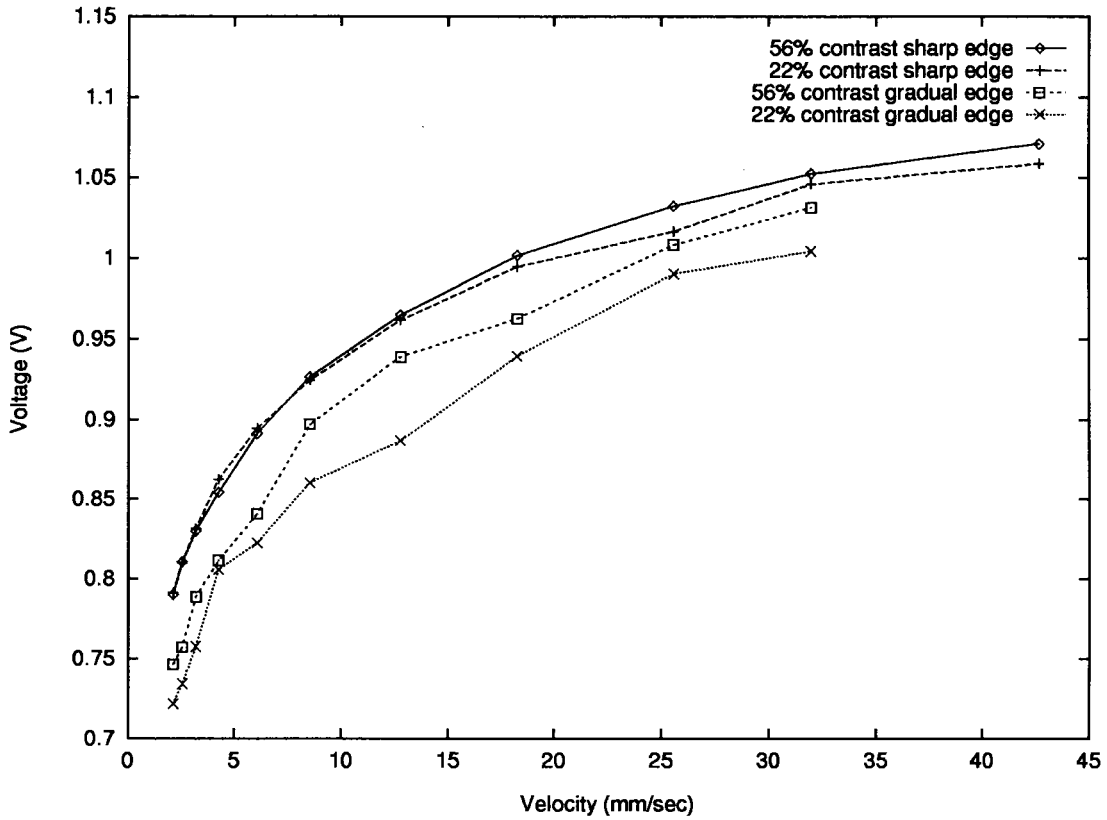

(b)

Fig. 8. Output signal of a motion sensing element for the preferred direction of motion of different ON edge stimuli versus image velocity for ac-incandescent room illumination. The data shows the contrast-dependence of the velocity measurements. Each data point represents the average of 5 successive measurements: (a) FT. (b) FS.

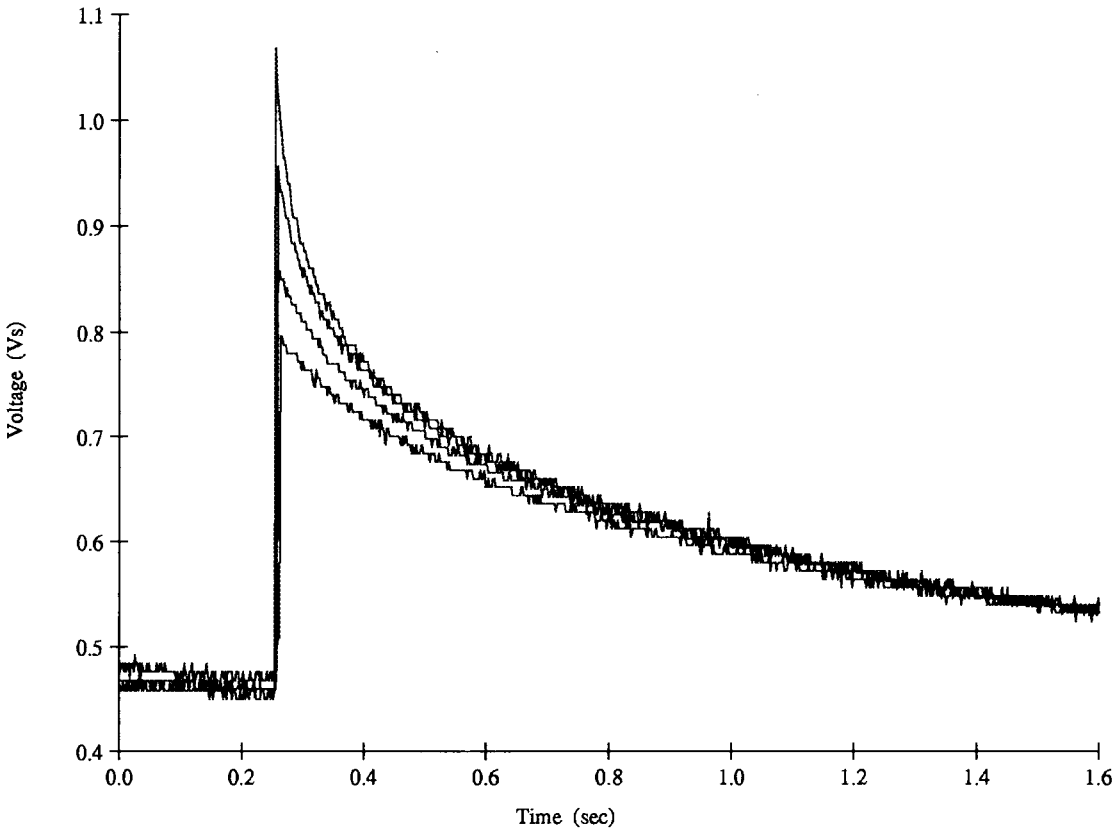

Fig. 9. Measured waveforms of the slowly-decaying voltage pulse V_s of an FSmotion sensing element in response to sharp edges of different contrasts. The four waveforms represent the response to edges with 56, 16, 11, and 5% contrast, respectively. The pulse amplitude monotonically decreases with contrast, but for sufficiently long times after their onset, all curves converge to a contrast-independent encoding of time delay and thus velocity. The noise level is smaller than the 10 mV quantization step of the measurements.

independent of speed and so does the output voltage of the velocity sensor [30]. Fig. 8(a) and (b) shows the effect of using different edge sharpnesses and contrasts for the FT and FS circuits, respectively. We define here edge contrast as the ratio of the difference and the sum of maximum and minimum irradiance. The decreased and more jagged response at lower contrasts and to more gradual edges can be explained by the smaller and broader current pulses generated by the edge detectors. The FT circuit is somewhat more invariant against edge contrast than the FS circuit. The response of the FS circuit to sharp edges is reasonably contrast-invariant down to contrasts of approximately 15%. For lower contrasts, the response gradually decreases [30], since the condition of (10) does not hold anymore. Fig. 9 shows how the measured traces of the timing pulses V_s for different contrasts converge to the same voltage—very quickly for high contrasts and slowly for low contrasts. The detection limit is at about 5% contrast. If dc illumination is used, there is no 120 Hz flicker noise, allowing the gain of the temporal edge detector to be increased by raising V_b. This further lowers the limits for contrast invariance and detection.

Fig. 10 shows the performance of the FS motion circuit if the edge detector is bypassed and the signals fed into the nonlinear filter (at V_{in} in Fig. 3(a)) are electronically-generated binary pulses. A theoretical fit, based on (6) is also plotted. The width of the input pulses was set to 50 μs. Spurious response in the null direction was observed for time delays smaller than the pulsewidth of the sampling signal V_f that was measured to be 5.3 μs. The sampled output voltage is a monotonic function of time delay and thus simulated velocity over at least seven orders of magnitude. The output voltage is a logarithmic function of velocity except for small time delays, where the condition of (10) is not satisfied, and for large time delays, where the voltage decays because of parasitic leak currents to ground.

In the low-gain mode used for ac illumination to suppress flicker noise, the amplifier of the edge detector is operated above threshold and the power consumption of both motion sensors is about 1 mW per element in a 1-D array. For dc illumination the amplifier can be operated in the subthreshold domain and the power consumption decreases to less than 100 μW per pixel.

VIII. Discussion

The facilitate-and-trigger (FT) and facilitate-and-sample (FS) motion sensors both unambiguously encode 1-D velocity, i.e., speed and direction of motion, over a considerable range. The outputs are quite insensitive to changes in global illumination over at least two orders of magnitude and also to edge contrast for higher spatial contrasts. For lower contrasts, the response gradually decreases with contrast.

The FS sensor exhibits desirable response characteristics in that it operates down to very low speeds, while maintaining a good sensitivity at higher speeds. For an ideal edge detector,

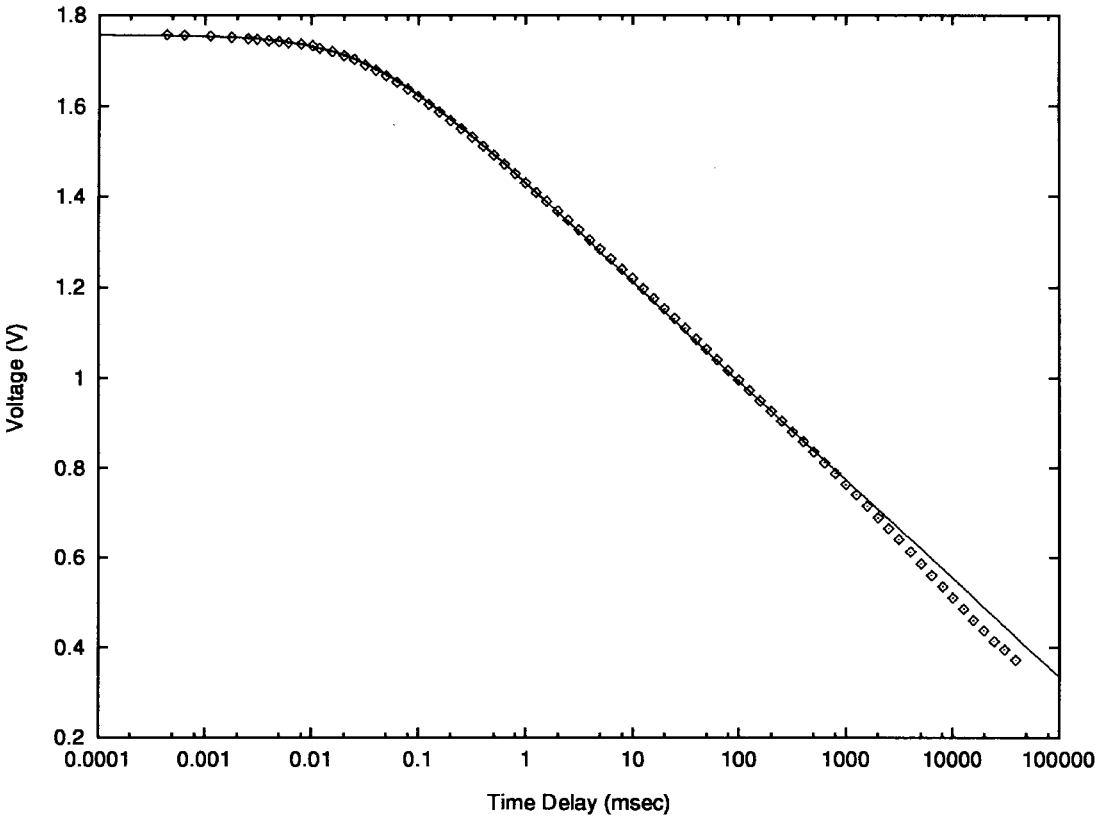

Fig. 10. Output voltage of an FS motion sensing element versus time delay for two 50 μs long electronic pulse inputs. The inputs simulate the outputs ofadjacent edge detectors for motion in the preferred direction. A theoretical fit based on (6) is also plotted. The rms error for each data point is less than1 mV. The FS motion sensor shows good performance over more than seven orders of magnitude of velocity for standardized input signals. A major improvement for the FS motion sensor would be the design of an edge detector providing such contrast-independent pulses.

the velocity range spans more than seven orders of magnitude. For the FT sensor, the time window T set by the facilitation pulse limits the minimum velocity that can be measured to $v_{\min} = \frac{\Delta x}{T}$ and the response curve rapidly saturates at high velocities. On the other hand, the FT sensor maintains its direction-selectivity up to very high speeds, while for the FS sensor, the finite width δt of the sampling pulse V_f limits the maximum velocity for direction-selectivity to $v_{\max} = \frac{\Delta x}{\delta t}$. For velocities smaller than $v_{\max}$, the FT sensor does not respond to motion in the null direction as long as the temporal separation of successive edges is larger than the sum of the delay time $\tau = \frac{\Delta x}{v}$ and the neuron pulsewidth T, whereas the FS sensor always samples the residual voltage from the facilitation pulse of the preceding edge in the null direction. If no spatial aliasing occurs, the response in the null direction due to temporal aliasing is always lower than that in the preferred direction for both circuits. A simple temporal anti-aliasing strategy to obtain zero response to motion in the null direction has been implemented [29]. It compares the outputs of a pair of motion circuits for opposite directions and suppresses the lower one. Alternatively, an inhibition scheme with three-pixel interaction can be used, as in [26].

The response of the FT circuit is somewhat less dependent on varying illumination and edge shapes than that of the FS ciruit. The full potential sensitivity of the edge detector, leading to contrast-invariant encoding of velocity down to lower spatial contrasts for both motion sensors, can only be exploited using dc illumination. Under ac lighting, the edge detector triggers spurious current pulses in response to the 120 Hz flicker noise, unless it is run at a low gain. Other options for the suppression of flicker noise include the limitation of the detector bandwidth, the use of a narrow-band filter, and the replacement of the temporal edge detector by a spatial edge detector [20], [23]. But spatial edge detectors tend to consume more silicon area and exhibit more offset problems, lower sensitivity, and slower response than the temporal edge detector described here.

Most of the previously reported analog VLSI motion sensors only respond robustly to high-contrast stimuli [10], [19], show a contrast-dependent output [14], [15], [18], [22], [25] or have a nonmonotonic response curve [14], [15], [18], [19], [22], [25]. A few implementations were reported to unambiguously encode velocity down to low contrasts [17], [23], [24], [26] but only for [26] results are given in the reference.

How can future motion sensors be improved? As witnessed by Fig. 10, using an ideal input stage that can robustly detect given image features and respond with standardized outputs (here mimicked by electronically-generated pulses) allows the FS motion circuit to have a reliable voltage response over at least seven orders of magnitude in velocity. The problem in the real world is that "features," whether temporal edges, spatial edges, or higher level features, are difficult to detect over a large contrast and illumination range. We believe that the construction of a compact edge detector that *adapts* over time or space would go a long way toward the design of truly robust motion sensors.

Scaling in One and Two Dimensions: An elementary cell of a 1-D motion sensor consists of an edge detector, a pulse-shaping circuit and two motion circuits. For the FT circuit, such a cell has 40 transistors and a total of 6.5 pF capacitance, whereas an FS cell comprises 30 transistors and 7.5 pF capacitance. For both circuits, the total area consumption is about 0.05 mm^2, if they are implemented using 2 μm CMOS technology. The smallest chips ("tiny" chips) available through MOSIS for the used process with an available area of about 2.5 mm^2 for the array (leaving room for read-out circuitry and pads) can accomodate 50 pixels. The largest chip would be able to contain 1250 pixels on 62.5 mm^2.

For an arrangement of elementary motion cells operating in two dimensions, the edge detectors and the pulse-shaping circuits may be shared among all directions, but each cell would need four motion circuits, one for each direction. This would increase the cell size by about 35%. If the circuits were fabricated in a state-of-the-art 0.7 μm process, the cells could probably be reduced to about a quarter of their current size, so that a 128 $\times$ 128 array would fit onto 16 mm $\times$ 16 mm chip area.

Such dense arrays of motion sensors would allow us to estimate extended optical flow fields and to extract certain qualitative features from them, such as time to contact, focus of expansion and motion discontinuities. We already implemented single-chip prototype systems that perform these functions with low resolution [31], [32].

IX. Conclusion

Two algorithms for the measurement of velocity in one dimension and their implementations with analog circuitry using CMOS VLSI technology were presented. The circuits are more compact and more reliable than most previously-reported analog, single-chip velocity sensors. They encode velocity robustly across a large range over two orders of magnitude of global illumination and are contrast-invariant for sufficiently high contrasts, while their response degrades gracefully at low contrasts.

Acknowledgment

Fabrication of the integrated circuits was provided by MOSIS.

References

[1] C. Koch and H. Li, Eds., *Vision Chips: Implementing Vision Algorithms With Analog VLSI Circuits*. Los Alamitos, CA: IEEE Computer Science Press, 1994.

[2] E. R. Fossum "Architectures for focal plane image processing," *Optical Eng.*, vol. 28, pp. 865–871, Aug. 1989.

[3] T. Poggio, W. Yang, and V. Torre, "Optical flow: Computational properties and networks, biological and analog," in *The Computing Neuron*, R. Durbin, C. Miall, and G. Mitchison, Eds. Wokingham, UK: Addison-Wesley, 1989, pp. 355–370.

[4] E. Vittoz and J. Fellrath, "CMOS analog integrated circuits based on weak inversion operation," *IEEE J. Solid-State Circuits*, vol. SC-12, pp. 224–231, June 1977.

[5] C. A. Mead, *Analog VLSI and Neural Systems*. Reading, MA: Addison-Wesley, 1989.

[6] J. Kramer, R. Sarpeshkar, and C. Koch, "An analog VLSI velocity sensor," in *Proc. 1995 IEEE Int. Symp. Circuits Syst.*, 1995, pp. 413–416.

[7] E. C. Hildreth and C. Koch, "The analysis of visual motion: From computational theory to neuronal mechanisms," *Ann. Rev. Neurosci.*, vol. 10, pp. 477–533, 1987.

[8] T. Poggio, V. Torre, and C. Koch "Computational vision and regularization theory," *Nature*, vol. 317, pp. 314–319, Sept. 1985.

[9] A. Verri and T. Poggio, "Motion field and optical flow: Qualitative properties," *IEEE Trans. Patt. Anal. Mach. Intell.*, vol. 11, pp. 490–498, May 1989.

[10] J. Tanner and C. Mead, "An integrated analog optical motion sensor," in *VLSI Signal Processing, II*, S. Y. Kung, R. E. Owen, and J. G. Nash, Eds. New York: IEEE Press, 1986, pp. 59–76.

[11] R. F. Lyon and M. P. Haeberli, "Designing and testing the optical mouse," *VLSI Design*, vol. 3, pp. 20–30, Jan./Feb. 1982.

[12] C. Koch, A. Moore, W. Bair, T. Horiuchi, B. Bishofberger, and J. Lazzaro, "Computing motion using analog VLSI vision chips: An experimental comparison among four approaches," in *Proc. IEEE Wkshp. Visual Motion*, Princeton, NJ, Oct. 1991, pp. 312–324.

[13] B. Hassenstein and W. Reichardt, "Systemtheoretische analyze der Zeit-, Reihenfolgen- und Vorzei-chenauswertung bei der Bewegungsperzeption des Rüsselkäfers chlorophanus," *Z. Naturforsch.*, vol. 11b, pp. 513–524, 1956.

[14] A. G. Andreou, K. Strohbehn, and R. E. Jenkins, "Silicon retina for motion computation," in *Proc. 1991 IEEE Int. Symp. Circuits Syst.*, Singapore, June 1991, pp. 1373–1376.

[15] R. C. Meitzler, K. Strohbehn, and A. G. Andreou, "A Silicon retina for 2-D position and motion computation," in *Proc. 1995 IEEE Int. Symp. Circuits Syst.*, 1995, pp. 2096–2099.

[16] S.-C. Liu, "Silicon model of motion adaptation in the fly visual system," in *Proc. 3rd Joint Caltech/UCSD Symp. Neural Comp.*, Pasadena, CA, June 1996.

[17] T. Horiuchi, J. Lazzaro, A. Moore, and C. Koch, "A delay line based motion detection chip," in *Advances in Neural Information Processing Systems 3*, R. Lippman, J. Moody, and D. Touretzky, Eds. San Mateo, CA: Morgan Kaufmann, 1991, pp. 406–412.

[18] T. Delbrück, "Silicon retina with correlation-based, velocity-tuned pixels," *IEEE Trans. Neural Networks*, vol. 4, pp. 529–541, May 1993.

[19] R. Sarpeshkar, W. Bair, and C. Koch, "Visual motion computation in analog VLSI using pulses," in *Advances in Neural Information Processing Systems 5*, D. S. Touretzky, Ed. San Mateo, CA: Morgan Kaufmann, 1993, pp. 781–788.

[20] W. Bair and C. Koch, "An analog VLSI chip for finding edges from zero-crossings," in *Advances in Neural Information Processing Systems 3*, R. Lippman, J. Moody, and D. Touretzky, Eds. San Mateo, CA: Morgan Kaufman, 1991, p. 399–405.

[21] H. B. Barlow and W. R. Levick, "The mechanism of directionally selective units in the rabbit's retina," *J. Physiol.*, vol. 178, pp. 447–504, 1965.

[22] R. G. Benson and T. Delbrück, "Direction selective silicon retina that uses null inhibition," in *Advances in Neural Information Processing Systems 4*, J. E. Moody, S. J. Hanson, and R. P. Lippmann, Eds., San Mateo, CA: Morgan Kaufmann, 1992, pp. 756–763.

[23] R. Etienne-Cummings, S. Fernando, N. Takahashi, V. Shtonov, J. Van der Spiegel, and P. Mueller, "A new temporal domain optical flow measurement technique for focal plane VLSI implementation," in *Proc. Comp. Arch. Mach. Perception 1993*, M. Bayoumi, L. Davis, and K. Valavanis, Eds. Piscataway, NJ: IEEE Press, 1993, pp. 241–250.

[24] R. Etienne-Cummings, "Biologically motivated analog VLSI systems for optomotor tasks," Ph.D. dissertation, Department of Electrical Engineering, University of Pennsylvania, Philadelphia, PA, 1994.

[25] P.-F. Rüedi, "Motion detection silicon retina based on event correlations," in *Proc. 5th Int. Conf. Microelectronics for Neural Networks and Fuzzy Systems*. Los Alamitos, CA: IEEE Computer Society Press, 1996, pp. 23–29.

[26] J. Kramer, "Compact integrated velocity sensor with three-pixel interaction," *IEEE Trans. Patt. Anal. Mach. Intell.*, vol. 18, pp. 455–460, Apr. 1996.

[27] T. Delbrück, "Investigations of analog VLSI visual transduction and motion processing," Ph.D. dissertation, Dep. Computat. Neural Syst., California Inst. Technol., Pasadena, CA, 1993.

[28] R. Sarpeshkar, L. Watts, and C. Mead, "Refractory neuron circuits," CNS Tech. Rep., CNS-TR-92-08, Calif. Inst. Technol., Pasadena, 1992.

[29] R. Sarpeshkar, J. Kramer, G. Indiveri, and C. Koch, "Analog VLSI architectures for motion processing: From fundamental limits to system applications," *Proc. IEEE*, vol. 84, pp. 969–987, July 1996.

[30] J. Kramer, G. Indiveri, and C. Koch, "Analog VLSI motion projects at Caltech," in *Proc. EUROPTO Conf. Advanced Focal Plane Arrays and Electronic Cameras*, Berlin, Germany, Oct. 1996, to be published.

[31] G. Indiveri, J. Kramer, and C. Koch, "Parallel analog VLSI architectures

for computation of heading direction and time-to-contact," in *Advances in Neural Information Processing Systems 8*, D. S. Touretzky, M. C. Mozer, and M. E. Hasselmo, Eds. Cambridge, MA: MIT Press, 1996, pp. 720–726.

[32] J. Kramer, R. Sarpeshkar, and C. Koch, "Analog VLSI motion discontinuity detectors for image segmentation," in *Proc. 1996 IEEE Int. Symp. Circuits Syst. II*, 1996, pp. 620–623.

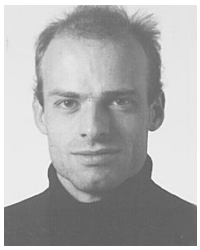

Jörg Kramer graduated in physics from the Swiss Federal Institute of Technology Zurich (ETHZ) in 1987, and received the M.S. degree in applied optics from Imperial College, London, in 1988. In 1993 he received the Ph.D. degree in physics from ETHZ for a project in optoelectronics carried out at the Paul Scherrer Institute Zurich.

Since then he has been a post-Doctoral fellow with the California Institute of Technology, working on analog VLSI vision systems.

Rahul Sarpeshkar was born in Bangalore, India, in 1968. He received a double major in electrical engineering and physics from the Massachusetts Institute of Technology in 1990. His bachelor's thesis research was on sense amplifiers in DRAM's, and was conducted at the T. J. Watson Research Center, IBM and at MIT. Since 1990 he has been a Ph.D. student in Carver Mead's analog VLSI Laboratory, California Institute of Technology, working on the design of wide-dynamic-range silicon cochleas.

While at the California Institute of Technology, he has done work on noise in devices, circuits and systems, on adaptive silicon cochleas, and in visual motion detection. His interests lie in analog circuit design for sensory systems, and in the fundamental limits of computing due to physics. He has authored 11 publications and holds one patent.

Dr. Sarpeshkar's bachelor's degree thesis won an award at MIT. He is a member of Tau Beta Pi and Sigma Pi Sigma.

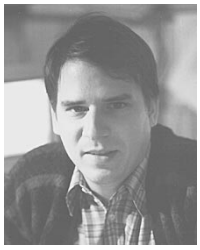

Christof Koch received the Ph.D. degree in biophysics in Tübingen, Germany.

After graduation, he spent four years at MIT's Artificial Intelligence Laboratory before moving to Caltech, where he has remained since 1986. Currently, he is a Professor of Computation and Neural Systems at the Institute. His research focuses on understanding the biophysical mechanisms underlying information storage and processing in single neurons, in particular the computations underlying motion and visual attention in cortical networks in the mammalian visual system. His laboratory builds neuromorphic, analog, smart vision chips to solve a host of applied vision problems. Together with Dr. F. Crick, he works on the neuronal basis of visual awareness and consciousness. He has published three books, more than one hundred technical articles, and has numerous patents in the area of vision chips.